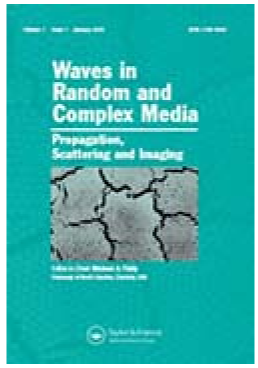

Effects of polymer's viscoelastic properties and curved shape of the CNTs on dynamic response of hybrid nanocomposite beams

Journal:	*Waves in Random and Complex Media*
Manuscript ID	TWRM-2021-0931.R1
Manuscript Type:	Regular Paper
Keywords:	Multi-scale hybrid nanocomposite, Viscoelastic material, Waviness, CNT-reinforced polymer, Vibration analysis

Effects of polymer's viscoelastic properties and curved shape of the CNTs on dynamic response of hybrid nanocomposite beams

Farzad Ebrahimi[1*], Reza Nopour[1], and Ali Dabbagh[2†]

[1] Department of Mechanical Engineering, Faculty of Engineering, Imam Khomeini International University, Qazvin, Iran
[2] School of Mechanical Engineering, College of Engineering, University of Tehran, Tehran, Iran

Abstract

Carbon nanotube (CNT)-reinforced polymer nanocomposites possess marvelous stiffness and strength as well as viscoelastic nature due to the time-dependent properties of the polymers. Hence, adequate knowledge about their rheological behavior is required if it is aimed at using such nanomaterials in design of aerospace structures. Present manuscript is arranged to account for the time-dependency of the polymer and wavy shape of the CNTs while tracking the vibrational responses of multi-scale hybrid nanocomposites for the first time. To this purpose, a combination of modified Halpin-Tsai model and mixture's rule is used for the homogenization process. According to dynamic form of the virtual work's principle, the governing equations will be attained based on a refined shear deformable beam theorem. In addition, the Galerkin's analytical solution is implemented to extract the system's natural frequency for both simply supported and clamped beams. The findings of this paper indicate on the fact that vibration suppression in the nanocomposite structures can be delayed if a high value is assigned to the polymer's relaxation time. Besides, it is illustrated that hybrid nanocomposites consisted of wavy CNTs cannot provide ideal frequencies related to the nanocomposites manufactured from straight CNTs.

Keywords: Multi-scale hybrid nanocomposite; Viscoelastic material; Waviness; CNT-reinforced polymer; Vibration analysis

1. Introduction

* Corresponding author, E-mail: febrahimy@eng.ikiu.ac.ir
† Corresponding author, E-mail: ali.dabbagh@ut.ac.ir

Since invention of carbon nanotubes (CNTs) in 1990s [1], a new window in science and technology was opened. As the gift of this opening, nanotechnology was born. Nanostructured materials showed astonishing material properties [2, 3] which satisfied the demands of engineering designs. Therefore, they were rapidly employed in different engineering aspects for design of critical devices. For instance, the ultra-high stiffness and strength of the CNTs as well as their incredible thermal and electrical conductivity led to their use in composites as reinforcements. Composites reinforced with nanoparticles, also known as nanocomposites, are now hired in different disciplines of engineering such as mechanics, automotive, aerospace, electronics, civil, etc. [4]. Nanocomposites can be categorized in three major groups of polymer nanocomposites (PNC), ceramic nanocomposites (CNCs), and metal nanocomposites (MNCs) based on their host material. Focusing on PNCs due to their light weight, several studies can be found in the literature concerned with investigation of structural performance of such nanocomposite structures [5-48]. However, all of these works employed simple micromechanical methods to find mechanical properties of PNCs. In other words, the CNTs are considered to be straight nanofillers which are distributed in the matrix in a uniform manner. These assumptions are in serious conflict with what appears in practice. In other words, CNTs are always shaped in non-straight forms and cannot be found individually in the nanocomposites. Researches have reported high possibilities of essence of a curved shape in the CNTs [49, 50]. Besides, bundles of CNTs are available in the nanocomposites instead of their single ones due to high van der Waals potential between them [50].

In the first years of 2010s, a group of Iranian researchers could present a semi-empirical model for homogenization of CNT-reinforced (CNTR) nanocomposites. In this method, decreasing effect of waviness phenomenon on the Young's modulus of CNTR nanocomposite was captured efficiently [51]. In this study, a simplified low-cost computational method was introduced which was able to estimate the modulus of CNTR nanocomposites with a limited reinforcement loading. After some years, another group consisted of Spanish scientists developed a micromechanical method to derive the material properties of CNTR nanocomposites with regard to the influence of curvy shape of the nanofillers on the modulus approximation. In this work, complicated algebra of tensors was hired to attain the modulus [52]. In comparison, the method introduced in Ref. [51] is superior to what recommended in Ref. [52] because it does not involve the user in high costs of computation.

The material properties of nanocomposites can be even better if multi-scale reinforcements are implemented in the fabrication. Suppose a nanocomposite that is hosted by a polymeric matrix and reinforced with macroscale fibers of carbon and CNT. Because of this composition, this kind of nanocomposites is called multi-scale hybrid (MSH) nanocomposite. Since the middles of 2010s, detailed studies about static and dynamic behaviors of MSH nanocomposite structures have been performed. Nonlinear frequency of free oscillations in multi-layered plates made from smart piezoelectric MSH nanocomposites was gathered in Ref. [53]. The impact of viscose losses on the nonlinear dynamic characteristics of viscoelastic MSH nanocomposite beams was studied in Ref. [54]. In another study, the influence of rotation of MSH nanocomposite blades on nonlinear mechanical response of this kind of nanocomposite structures was captured [55]. Later, Iranian researchers made an effort to analyze the reaction of MSH nanocomposite plates to hygro-thermo-elastically excited low-velocity impact stimulation [56]. Moreover, the effect of utilization of graphene platelets (GPLs) in the composition of MSH nanocomposites on nonlinear bending, post-buckling temperature, and bifurcation path of beam-type structures was reported in Ref. [57]. In another endeavor, modal behaviors of thick beams made from MSH nanocomposites reinforced via graphene oxide were monitored in the context of finite element method (FEM) [58]. Buckling resistance of MSH nanocomposite plates reinforced via entangled nanofillers was probed in Ref. [59] via an analytical approach. Moreover, the issue of studying free vibration problem in cylindrical shells made from MSH nanocomposites was payed attention in Ref. [60]. In a similar atmosphere, nonlinear stability paths of MSH nanocomposite thin beams with initial imperfection were attained and interpreted in Ref. [61]. With the aid of beams' HSDT, both elastic and thermo-mechanical buckling resistances of MSH nanocomposite beams were surveyed in Refs. [62] and [63], respectively. On the other hand, Kirchhoff-Love theory of thin rectangular plates was utilized in Ref. [64] for the goal of investigating critical buckling load of MSH nanocomposite plates. Using HSDT of thick plates, the same research group explored the influence of nanofillers' aggregation on the natural frequency of MSH nanocomposite plates [65].

Even though invaluable efforts have been made by now toward analyzing MSH nanocomposite structures, the time-varying modulus of polymer is disregarded in most of the accomplished studies. This assumption, however, makes the analysis far from the real circumstance. We know that polymers encompass a rheological behavior and their modulus varies as time exceeds. With regard to this issue, damped dynamic behaviors of hybrid nanocomposite plates were reported in

Ref. [66]. Except this study, no other work about dynamic performance of MSH nanocomposite structures can be addressed. So, it is easy to realize that there exists no data about dynamic responses of viscoelastic MSH nanocomposite beams while the effect of waviness phenomenon on the system's response is covered. Based on the broad applications of nanocomposites in structural mechanics (see Figure 1) and to compensate the existing lack, the authors decided to analyze the damped vibration problem of thick beams made from MSH nanocomposites made from curved CNTs. In the what follows, a big section is presented to derive the equivalent properties of the viscoelastic nanocomposite. Then, kinematic relations are provided for thick beams. Once the governing equations are gathered, the problem will be solved with the aid of Galerkin's method for MSH nanocomposite beams with simply support and clamped ends.

2. Theory and formulation

2.1. Micromechanical homogenization

In this part, the material properties of MSH nanocomposite will be derived in a hierarchical procedure. First of all, the properties of polymer will be explored. Polymers exhibit viscoelastic material behavior. Such soft materials are usually characterized by their long-term mechanical behavior due to their viscoelastic nature [67]. In general, polymers manifest a nonlinear behavior from themselves in the time domain. Therefore, their rheological features must be captured by regarding for the gradual changes in their compliance (or stiffness) as time exceeds [68]. In this research, mechanical properties of the polymeric matrix, namely E_{PM} and ν_{PM}, are presumed to be time-dependent with according to an exponential function of time. Based on the Maxwell model [69, 70], Young's modulus of the polymers can be presented in the following form:

$$E_{PM}(t) = E_{PM}^{0} \exp\left(-\frac{t}{\tau_v}\right)^{\beta_v} \tag{1}$$

where E_{PM}^{0} is the instantaneous elastic modulus at the initial time. The parameters β_v and τ_v are the stretching exponent and characteristic relaxation time, respectively [70]. Similarly, the Poisson's ratio can be presumed to be in the below time-dependent form [70]:

$$\nu_{PM}(t) = 0.5 - (0.5 - \nu_{PM}^{0}) \exp\left(-\frac{t}{\tau_v}\right)^{\beta_v} \tag{2}$$

in which ν_{PM}^{0} represents the initial value of Poisson's ratio. It should be remembered that the polymer's density is not time-dependent; therefore, $\rho_{PM}^{0} = \rho_{PM}$.

Now, the material properties of the polymer matrix are in hand and it is time to go through finding the effective material properties of CNTR nanocomposites. To this purpose and with regard to the negative influence of existence of wavy CNTs on the total stiffness of the nanocomposite material, the modified form of the Halpin-Tsai [51] will be utilized. The aforementioned model can be utilized in the cases that lower than 2% of the nanocomposite's volume is dedicated to reinforcing CNTs. In the mentioned domain, results of this model were proven to be in accordance with those achieved from the experiments [51]. Based on this method, the Young's modulus of the CNTR nanocomposite can be written as below:

$$E_{NCM} = \frac{1 + C\eta V_{CNT}}{1 - \eta V_{CNT}} E_{PM} \tag{3}$$

where

$$\eta = \frac{C_w \left[\alpha \, E_{CNT} / E_{PM} \right] - 1}{C_w \left[\alpha \, E_{CNT} / E_{PM} \right] + C} \tag{4}$$

In the above equation, the term α is the factor of orientation introduced in Ref. [71]. Also, C is the size-dependent coefficient equal to two times the ratio between the length and the diameter of the CNTs. α is considered equal to $1/6$ because length of the CNTs is small compared to the total thickness of the structure (i.e. in the range of millimeters) [71]. Besides, C_w is the waviness coefficient and can be varied from zero to one. The expression of the waviness coefficient is $C_w = 1 - a/w$ while the amplitude of the existing wave in the structure of the CNT is shown with a and the w denotes half of the direct distance between two ends of a wavy CNT. Further explanation about the way in which this coefficient is derived can be completely found by referring to Ref. [51]. In fact, this coefficient will define the amplitude of the wave produced by the CNTs' curvature. In other words, if this coefficient is considered to be at its upper limit, all CNTs are straight. The half-circle shape of the CNTs can also be imagined when the waviness factor is assumed to be zero. The mass density and Poisson's ratio of the CNTR nanocomposite can be derived using the definition of rule of the mixture [71]:

$$\rho_{NCM} = \rho_{CNT}V_{CNT} + \rho_{PM}V_{PM} \tag{5}$$

$$\nu_{NCM} = \nu_{CNT}V_{CNT} + \nu_{PM}V_{PM} \tag{6}$$

Combining definitions presented in Eqs. (3) and (6), shear modulus of the CNTR nanocomposite can be presented as below:

$$G_{NCM} = \frac{E_{NCM}}{2\left(1+\nu_{NCM}\right)} \tag{7}$$

In Eqs. (3), (5), and (6), the volume fraction of the CNTs in the CNTR nanocomposite can be calculated using the following definition [70]:

$$V_{CNT} = \left(\frac{\rho_{CNT}}{m_r\rho_{PM}} - \frac{\rho_{CNT}}{\rho_{PM}} + 1\right)^{-1} \tag{8}$$

where ρ_{CNT} and ρ_{PM} are the mass densities of CNTs and polymer matrix, respectively. In addition, m_r is the mass fraction of the reinforcing phase, i.e. CNT.

Now, material properties of the MSH nanocomposite can be achieved. To this end, the CNTR nanocomposite (with material properties presented in Eqs. (3), (5)-(7)) must be considered as the matrix of a composite material whose reinforcing agent is glass fiber (GF). The reinforcing fibers are characterized by the corresponding Young's modulus E_F, shear modulus G_F, and Poisson's ratio ν_F. Herein, the fibers are considered to be isotropic solids. The volume fraction of GFs can be determined using the below expression [70]:

$$V_F = \left(\frac{\rho_F}{m_f\rho_{NCM}} - \frac{\rho_F}{\rho_{NCM}} + 1\right)^{-1} \tag{9}$$

in which the mass density of fibers is shown with ρ_F and m_f corresponds with the mass fraction of the fibers. The mechanical properties of the MSH nanocomposite can be assessed implementing the rule of the mixture as follows [70]:

$$E_{11} = E_F V_F + E_{NCM} V_{PM}^{*} \tag{10}$$

$$G_{13} = \frac{G_{NCM}}{1 - V_F(1 - G_{NCM} / G_F)} \tag{11}$$

2.2. Refined higher-order beam theory

In this section, the kinematic relations needed to derive the components of strain tensor of the continuous system will be presented. Because of the fact that this study is proposed to probe thick-type nanocomposite beams, a refined shear deformable beam model is utilized. According to this type of the beam theories, the displacement field of the structure can be described as below [4]:

$$\begin{aligned} &u_x(x,z,t) = u(x,t) - z\frac{\partial w_b(x,t)}{\partial x} - f(z)\frac{\partial w_s(x,t)}{\partial x}, \\ &u_y(x,z,t) = 0, \\ &u_z(x,z,t) = w_b(x,t) + w_s(x,t) \end{aligned} \tag{12}$$

where u represents the axial displacement of the neutral axis of the beam. The deflections caused by bending and shear modes are shown with w_b and w_s, respectively. Also, $f(z)$ stands for the shape function i.e. aimed at controlling the profile of the shear strain and stress across the thickness direction. In this study, the shape function introduced in Ref. [72] is implemented. Now, the components of the strain tensor can be attained with the aid of the following definition provided in Ref. [73] for the infinitesimal strains:

$$\varepsilon_{ij} = \frac{1}{2}\left(u_{i,j} + u_{j,i}\right) \tag{13}$$

It should be recalled that ε_{ij} denotes the components of the 4th-order strain tensor. Also, $u_{i,j}$ represents the derivation of u_i component of displacement field with respect to x_j component of the cartesian coordinate system. Now, the nonzero strains of the system can be presented in the following form if Eq. (12) is inserted into Eq. (13):

$$\varepsilon_{xx} = \frac{\partial u}{\partial x} - z\frac{\partial^2 w_b}{\partial x^2} - f(z)\frac{\partial^2 w_s}{\partial x^2}, \;\; \gamma_{xz} = g(z)\frac{\partial w_s}{\partial x} \tag{14}$$

where $g(z) = 1 - df(z)/dz$.

2.3. Motion equations

The well-known Hamilton's principle will be employed in this section in order to derive the motion equations of the beam-type element. The mathematical definition of this principle in general form can be written as below [4]:

$$\int_{0}^{t} \delta(U - T + V)dt = 0 \tag{15}$$

where U, T, and V stand for the strain energy, kinetic energy, and work done by external loading, respectively. Now, the variations of each of the aforementioned energies must be determined accordingly. First, the variation of the strain energy can be shown in the following form [4]:

$$\delta U = \int_{\forall} \left(\sigma_{xx} \delta\varepsilon_{xx} + \sigma_{xz} \delta\gamma_{xz} \right) d\forall \tag{16}$$

In the above definition, $\forall$ is the total volume of the continuous system. By substituting for the strain components from Eq. (14) into the above definition, the variation of the strain energy can be re-written in the following form:

$$\delta U = \int_{0}^{L} \left(N \frac{\partial \delta u}{\partial x} - M_b \frac{\partial^2 \delta w_b}{\partial x^2} - M_s \frac{\partial^2 \delta w_s}{\partial x^2} + Q \frac{\partial \delta w_s}{\partial x} \right) dx \tag{17}$$

In the above relation, the stress resultants can be presented in the following form:

$$\begin{aligned} &[N, M_b, M_s] = \int_{A} [1, z, f(z)] \sigma_{xx} dA, \\ &Q = \int_{A} g(z) \sigma_{xz} dA \end{aligned} \tag{18}$$

Besides, the variation of the kinetic energy of the system can be described in the following form [4]:

$$\delta T = \int_{\forall} \left(\frac{\partial u_x}{\partial t} \frac{\partial \delta u_x}{\partial t} + \frac{\partial u_z}{\partial t} \frac{\partial \delta u_z}{\partial t} \right) \rho d\forall \tag{19}$$

Once Eq. (12) is inserted into the above definition, the variation of the kinetic energy can be re-written as below:

$$\delta T = \int_0^L \begin{bmatrix} I_0\left(\frac{\partial u}{\partial t}\frac{\partial \delta u}{\partial t}+\frac{\partial (w_b+w_s)}{\partial t}\frac{\partial \delta (w_b+w_s)}{\partial t}\right)-I_1\left(\frac{\partial u}{\partial t}\frac{\partial^2 \delta w_b}{\partial x\partial t}+\frac{\partial^2 w_b}{\partial x\partial t}\frac{\partial \delta u}{\partial t}\right) \\ -J_1\left(\frac{\partial u}{\partial t}\frac{\partial^2 \delta w_s}{\partial x\partial t}+\frac{\partial^2 w_s}{\partial x\partial t}\frac{\partial \delta u}{\partial t}\right)+I_2\frac{\partial^2 w_b}{\partial x\partial t}\frac{\partial^2 \delta w_b}{\partial x\partial t}+K_2\frac{\partial^2 w_s}{\partial x\partial t}\frac{\partial^2 \delta w_s}{\partial x\partial t}+ \\ J_2\left(\frac{\partial^2 w_b}{\partial x\partial t}\frac{\partial^2 \delta w_s}{\partial x\partial t}+\frac{\partial^2 w_s}{\partial x\partial t}\frac{\partial^2 \delta w_b}{\partial x\partial t}\right) \end{bmatrix} dx \tag{20}$$

The cross-sectional mass moments of inertia utilized in the above relation can be calculated using the following definitions:

$$[I_0, I_1, J_1, I_2, J_2, K_2] = \int_A [1, z, f(z), z^2, zf(z), f^2(z)]\rho dA \tag{21}$$

According to the fact that there exists no external loading in the present problem (i.e. corresponding with $\delta V = 0$), the Euler-Lagrange equations of the beam can be obtained by substituting for the variations of the strain and kinetic energies from Eqs. (17) and (20), respectively into Eq. (15):

$$\frac{\partial N}{\partial x} = I_0\frac{\partial^2 u}{\partial t^2} - I_1\frac{\partial^3 w_b}{\partial x\partial t^2} - J_1\frac{\partial^3 w_s}{\partial x\partial t^2} \tag{22}$$

$$\frac{\partial^2 M_b}{\partial x^2} = I_0\frac{\partial^2 (w_b+w_s)}{\partial t^2} + I_1\frac{\partial^3 u}{\partial x\partial t^2} - I_2\frac{\partial^4 w_b}{\partial t^2\partial x^2} - J_2\frac{\partial^4 w_s}{\partial t^2\partial x^2} \tag{23}$$

$$\frac{\partial^2 M_s}{\partial x^2} + \frac{\partial Q}{\partial x} = I_0\frac{\partial^2 (w_b+w_s)}{\partial t^2} + J_1\frac{\partial^3 u}{\partial x\partial t^2} - J_2\frac{\partial^4 w_b}{\partial t^2\partial x^2} - K_2\frac{\partial^4 w_s}{\partial t^2\partial x^2} \tag{24}$$

2.4. Constitutive equations

In this part, elastic stress-strain relations of the nanocomposite material are depicted. According to the constitutive relations of linearly solids, the stress and strain tensors can be related to each other using the following definition [73]:

$$\boldsymbol{\sigma} = \mathbf{C} : \boldsymbol{\varepsilon} \tag{25}$$

in which $\boldsymbol{\sigma}$ and $\boldsymbol{\varepsilon}$ are the 2nd-order Cauchy stress and strain tensors, respectively. Also, $\mathbf{C}$ is the 4th-order tensor of elasticity. For beam-type elements, Eq. (25) can be summarized as below:

$$\sigma_{xx} = E_{11}\varepsilon_{xx}, \qquad \sigma_{xz} = G_{13}\gamma_{xz} \tag{26}$$

Once the above relations are integrated over the cross section area of the beam with regard to the definitions of the stress resultants previously mentioned in Eq. (18), the below relations between the stress resultants and displacement field of the nanocomposite beam can be achieved:

$$N = A\frac{\partial u}{\partial x} - B\frac{\partial^2 w_b}{\partial x^2} - B_s\frac{\partial^2 w_s}{\partial x^2} \tag{27}$$

$$M_b = B\frac{\partial u}{\partial x} - D\frac{\partial^2 w_b}{\partial x^2} - D_s\frac{\partial^2 w_s}{\partial x^2}, \tag{28}$$

$$M_s = B_s\frac{\partial u}{\partial x} - D_s\frac{\partial^2 w_b}{\partial x^2} - H_s\frac{\partial^2 w_s}{\partial x^2}, \tag{29}$$

$$Q = A_s\frac{\partial w_s}{\partial x}, \tag{30}$$

The cross-sectional rigidities used in Eqs. (27)-(30) can be computed using the below definitions:

$$\begin{aligned} &[A, B, D, B_s, D_s, H_s] = \int_A [1, z, z^2, f(z), zf(z), f^2(z)] E_{11} dA, \\ &A_s = \int_A g^2(z) G_{13} dA \end{aligned} \tag{31}$$

2.5. Governing equations

In this part, the mathematical formulation of the problem will be completed by substituting for the stress resultants from Eqs. (27)-(30) into the Euler-Lagrange equations formerly presented in Eqs. (22)-(24). Once the above substitution is accomplished, the governing equations of the nanocomposite beam can be presented in the below form:

$$A\frac{\partial^2 u}{\partial x^2} - B\frac{\partial^3 w_b}{\partial x^3} - B_s\frac{\partial^3 w_s}{\partial x^3} - I_0\frac{\partial^2 u}{\partial t^2} + I_1\frac{\partial^3 w_b}{\partial x \partial t^2} + J_1\frac{\partial^3 w_s}{\partial x \partial t^2} = 0 \tag{32}$$

$$B\frac{\partial^3 u}{\partial x^3} - D\frac{\partial^4 w_b}{\partial x^4} - D_s\frac{\partial^4 w_s}{\partial x^4} - I_0\frac{\partial^2 (w_b + w_s)}{\partial t^2} - I_1\frac{\partial^3 u}{\partial x \partial t^2} + I_2\frac{\partial^4 w_b}{\partial t^2 \partial x^2} + J_2\frac{\partial^4 w_s}{\partial t^2 \partial x^2} = 0 \tag{33}$$

$$B_s\frac{\partial^3 u}{\partial x^3} - D_s\frac{\partial^4 w_b}{\partial x^4} - H_s\frac{\partial^4 w_s}{\partial x^4} + A_s\frac{\partial^2 w_s}{\partial x^2} - I_0\frac{\partial^2 (w_b + w_s)}{\partial t^2} - J_1\frac{\partial^3 u}{\partial x \partial t^2} + J_2\frac{\partial^4 w_b}{\partial t^2 \partial x^2} + K_2\frac{\partial^4 w_s}{\partial t^2 \partial x^2} = 0 \tag{34}$$

3. Analytical solution

Till now, different approaches have been implemented by a wide range of researchers to probe mechanical behaviors of composites [74-79]. Here, the well-known Galerkin's method is used in order to solve the governing equations. According to this analytical method, the displacement field of the beam can be assumed to be in the following form [4]:

$$u(x,t) = \sum_{n=1}^{\infty} U_n \frac{\partial X_n(x)}{\partial x} e^{i\omega_n t},$$
$$w_b(x,t) = \sum_{n=1}^{\infty} W_{bn} X_n(x) e^{i\omega_n t}, \tag{35}$$
$$w_s(x,t) = \sum_{n=1}^{\infty} W_{sn} X_n(x) e^{i\omega_n t}$$

in which U_n, W_{bn}, and W_{sn} are the unknown Fourier coefficients regarding for the oscillation amplitudes. Also, X_n is a function which is arranged to satisfy the essential boundary conditions (BCs). In this study, nanocomposite beams with both ends either simply supported (S-S) or clamped (C-C) are probed. For the aforesaid BCs, the X_n function can be presented as below [4]:

$$\text{S-S}: \quad X_n(x) = \sin\left(\frac{n\pi}{L} x\right)$$
$$\text{C-C}: \quad X_n(x) = \sin^2\left(\frac{n\pi}{L} x\right) \tag{36}$$

Once Eq. (35) is substituted into Eqs. (32)-(34) and the orthogonality of the natural modes are considered, the following eigenvalue equation will be obtained [4]:

$$\mathbf{K}\boldsymbol{\Delta} = \mathbf{M}\omega_n^{\,2}\boldsymbol{\Delta} \tag{37}$$

in which $\mathbf{K}$ and $\mathbf{M}$ are respectively stiffness and mass matrices. Both of the aforementioned matrices are symmetric square matrices of order 3. In addition, the vector $\boldsymbol{\Delta}$ is the amplitude vector of free vibration of the system. By solving the above eigenvalue equation for ω_n, the natural frequency of system's fluctuation will be gathered.

4. Numerical results and discussion

This section is presented in order to discuss about the numerical results of this work. Material properties of polymer and GF are selected as same as those reported in Ref. [70] and can be found in Table 1. Also, the material properties of CNTs are gathered from Ref. [56] and are provided in Table 2 for the sake of completeness. In the following illustrations, thickness of the beam is assumed to be $h = 2$ mm and the slenderness ratio is fixed on $L/h = 10$ for the sake of considering the mechanical characteristics of thick-type structures. Moreover, the stretching component is fixed on $\beta_v = 1$ in all of the numerical results. On the other hand, the relaxation time is fixed on $\tau_v = 120$ sec unless another value is mentioned. In addition, the following dimensionless form of the natural frequency will be used in this study:

$$\Omega = \omega h \sqrt{\frac{\rho_{PM}^0}{E_{PM}^0}} \tag{38}$$

4.1. Validation study

Validity of the presented methodology is examined in this sub-section. To this end and in Table 3, natural frequency responses of CNTR nanocomposite beams are compared. According to this table, it can be realized that the present results are in an acceptable agreement with those reported in Refs. [9] and [80]. The tiny differences between the results are originated from the fact that Timoshenko beam model is utilized in Ref. [9] and the answers provided in Ref. [80] are extracted with the aid of the Rayleigh-Ritz FE solution. However, present study undergoes with an analytical solution incorporated with a refined-type HSDT. Furthermore, Table 4 is provided to confirm that the presented methodology can satisfy a reliable precision. According to this table, dynamic responses of nanocomposite beams with various nanoparticle loadings can be well estimated.

4.2. Influences of BC and relaxation time on the 1st natural frequency

Figure 2 is depicted for the purpose of plotting the variation of fundamental natural frequency of the MSH nanocomposite S-S and C-C beams against time whenever the characteristics time is changed. As shown in the figure, the decreasing trend of natural frequency will be postponed by increasing the relaxation time of the polymer matrix. This phenomenon can be justified by recalling the fact that increment of the relaxation time results in generation of a delay in the attenuation of the polymer's stiffness. Hence, it is natural to observe such a retardation in the time-frequency curve of the system. Furthermore, it can be understood that natural frequencies corresponding with C-C beams are approximately two times greater than those related to the S-S beams. The reason of this issue is the higher structural stiffness of the clamped-type support which leads to a geometrically stiffer system, as explained in Ref. [4].

4.3. Influences of the waviness phenomenon and CNTs' mass fraction on the 1st natural frequency

The time-frequency curve of three-phase hybrid nanocomposite structures with S-S BC for various amounts of the mass fraction of either straight or wavy CNTs is presented in Figure 3. According to this figure, it can be realized that waviness phenomenon can affect the time-frequency curve of the system in a remarkable manner. Indeed, existence of a wave in the shape of the CNTs results in reduction of the reinforcing power of the CNTs which leads to a decrease in the total stiffness of the MSH nanocomposite structure. Due to this fact, the natural frequency will be reduced. On the other hand, Figure 3 reveals that time-frequency curve can be shifted upward by making a small rise in the mass fraction of the CNTs. This trend appears thanks to exceptional stiffness of the CNTs which can cause noticeable enhancement in the system's dynamic response once the CNT loading in the composition of hybrid nanomaterial is aggrandized by only a limited value.

4.4. Influences of the waviness phenomenon and GFs' mass fraction on the 1st natural frequency

Similar to Figure 3, Figure 4 aims at investigating the impact of changing mass fraction of the GFs on the time-frequency curve of MSH nanocomposite S-S beams. It can be perceived that the same trends are valid in this case, too. The reason is of course the positive influence of the reinforcing GFs on entire stiffness of the three-phase nanomaterial. Actually, Young's modulus of the GFs is many times greater than that of the polymer matrix and this difference results in such a phenomenon. Once again, it is illustrated that nanocomposite structures consisted of wavy CNTs can provide smaller natural frequencies due to the negative effect of the waviness phenomenon on stiffness of the nanocomposite.

4.5. Influence of the waviness coefficient on the first three natural frequencies

The final example shown in Figure 5 indicates on the impact of selection of the waviness coefficient on approximation of the natural frequency in the first three natural modes. Based on this figure, an enhancement in value of the waviness coefficient results in a reciprocal upward shift in time-frequency curve in each of the natural modes. The reason is that increasing the waviness coefficient is corresponding with the consideration of essence of straighter CNTs in composition of the nanocomposite structure. So, it is not strange to see such an increasing trend because utilization of straight CNTs results in having stiffer nanocomposites. According to the experiments [51], implementation of waviness coefficients in the $0.3 < C_w < 0.4$ range can be resulted into obtaining results in agreement with those observed in the practical cases.

5. Conclusions

Present paper was arranged for the goal of probing the mechanical behaviors of three-phase polymer-GF-CNT nanocomposites with respect to wavy shape of the CNTs and viscoelastic nature of the polymer. The equivalent material properties were attained in the context of a tri-level hierarchical procedure. Afterward, governing equations were extracted with the aid of refined HSDT incorporated with dynamic form of the principle of virtual work. Natural frequencies of both S-S and C-C nanocomposite structures were derived by the means of Galerkin's analytical solution. Now, the most crucial highlights of this study will be reviewed again:

- Implementation of the waviness coefficient of $C_w = 0.35$ provides results close to those reported in the experimental examinations. This selection results in the complete consideration of the waviness phenomenon.
- An increase in the relaxation time leads to observing higher natural frequencies. Hence, it is recommended to utilize low relaxation times in the theoretical simulations to avoid from engineering overestimations.
- Once the wavy shape of the CNTs and the viscoelastic nature of the polymer matrix are dismissed, the natural frequencies of the system's free vibrations are many times higher than those happening in the practical applications. Therefore, the dynamic stability margin of the nanocomposite system cannot be determined thoroughly.
- It can be stated that dynamic behaviors of all of the first three modes will be affected by waviness phenomenon in the same manner.
- Presented modeling gives reliable data about viscoelastically damped vibrations of MSH nanocomposite thick beams free from any external shear correction coefficient.

Although present work possesses the abovementioned findings, it must be payed attention that some issues are dismissed in it. As a recommendation for future studies, investigation of the influence of agglomeration phenomenon on the damped dynamic behaviors of MSH nanocomposite beams can be addressed.

References

1. Iijima S. Helical microtubules of graphitic carbon. Nature. 1991; 354(6348):56-58.
2. Ruoff RS, Lorents DC. Mechanical and thermal properties of carbon nanotubes. Carbon. 1995; 33(7):925-930.
3. Xie S, Li W, Pan Z, et al. Mechanical and physical properties on carbon nanotube. Journal of Physics and Chemistry of Solids. 2000; 61(7):1153-1158.
4. Ebrahimi F, Dabbagh A. Mechanics of Nanocomposites: Homogenization and Analysis. 1st ed. Boca Raton, FL, USA: CRC Press; 2020.
5. Shen H-S, Zhang C-L. Thermal buckling and postbuckling behavior of functionally graded carbon nanotube-reinforced composite plates. Materials & Design. 2010; 31(7):3403-3411.
6. Shen H-S. Postbuckling of nanotube-reinforced composite cylindrical shells in thermal environments, Part II: Pressure-loaded shells. Composite Structures. 2011; 93(10):2496-2503.
7. Wang Z-X, Shen H-S. Nonlinear vibration of nanotube-reinforced composite plates in thermal environments. Computational Materials Science. 2011; 50(8):2319-2330.
8. Wang Z-X, Shen H-S. Nonlinear dynamic response of nanotube-reinforced composite plates resting on elastic foundations in thermal environments. Nonlinear Dynamics. 2012; 70(1):735-754.
9. Yas MH, Samadi N. Free vibrations and buckling analysis of carbon nanotube-reinforced composite Timoshenko beams on elastic foundation. International Journal of Pressure Vessels and Piping. 2012; 98:119-128.
10. Zhu P, Lei ZX, Liew KM. Static and free vibration analyses of carbon nanotube-reinforced composite plates using finite element method with first order shear deformation plate theory. Composite Structures. 2012; 94(4):1450-1460.
11. Lei ZX, Liew KM, Yu JL. Large deflection analysis of functionally graded carbon nanotube-reinforced composite plates by the element-free kp-Ritz method. Computer Methods in Applied Mechanics and Engineering. 2013; 256:189-199.
12. Rafiee M, Yang J, Kitipornchai S. Thermal bifurcation buckling of piezoelectric carbon nanotube reinforced composite beams. Computers & Mathematics with Applications. 2013; 66(7):1147-1160.
13. Ansari R, Faghih Shojaei M, Mohammadi V, et al. Nonlinear forced vibration analysis of functionally graded carbon nanotube-reinforced composite Timoshenko beams. Composite Structures. 2014; 113:316-327.
14. Shen H-S, Xiang Y. Postbuckling of axially compressed nanotube-reinforced composite cylindrical panels resting on elastic foundations in thermal environments. Composites Part B: Engineering. 2014; 67:50-61.
15. Zhang LW, Song ZG, Liew KM. Nonlinear bending analysis of FG-CNT reinforced composite thick plates resting on Pasternak foundations using the element-free IMLS-Ritz method. Composite Structures. 2015; 128:165-175.
16. Tornabene F, Fantuzzi N, Bacciocchi M, et al. Effect of agglomeration on the natural frequencies of functionally graded carbon nanotube-reinforced laminated composite doubly-curved shells. Composites Part B: Engineering. 2016; 89:187-218.
17. Duc ND, Cong PH, Tuan ND, et al. Thermal and mechanical stability of functionally graded carbon nanotubes (FG CNT)-reinforced composite truncated conical shells surrounded by the elastic foundations. Thin-Walled Structures. 2017; 115:300-310.
18. Ebrahimi F, Farazmandnia N. Thermo-mechanical vibration analysis of sandwich beams with functionally graded carbon nanotube-reinforced composite face sheets based on a higher-order shear deformation beam theory. Mechanics of Advanced Materials and Structures. 2017; 24(10):820-829.
19. Fantuzzi N, Tornabene F, Bacciocchi M, et al. Free vibration analysis of arbitrarily shaped Functionally Graded Carbon Nanotube-reinforced plates. Composites Part B: Engineering. 2017; 115:384-408.

20. Kamarian S, Bodaghi M, Pourasghar A, et al. Vibrational behavior of non-uniform piezoelectric sandwich beams made of CNT-reinforced polymer nanocomposite by considering the agglomeration effect of CNTs. Polymer Composites. 2017; 38(S1):E553-E562.
21. Memar Ardestani M, Zhang LW, Liew KM. Isogeometric analysis of the effect of CNT orientation on the static and vibration behaviors of CNT-reinforced skew composite plates. Computer Methods in Applied Mechanics and Engineering. 2017; 317:341-379.
22. Civalek Ö, Baltacıoğlu AK. Vibration of carbon nanotube reinforced composite (CNTRC) annular sector plates by discrete singular convolution method. Composite Structures. 2018; 203:458-465.
23. Kiani Y, Mirzaei M. Rectangular and skew shear buckling of FG-CNT reinforced composite skew plates using Ritz method. Aerospace Science and Technology. 2018; 77:388-398.
24. Moradi-Dastjerdi R, Aghadavoudi F. Static analysis of functionally graded nanocomposite sandwich plates reinforced by defected CNT. Composite Structures. 2018; 200:839-848.
25. Ansari R, Torabi J, Hassani R. A comprehensive study on the free vibration of arbitrary shaped thick functionally graded CNT-reinforced composite plates. Engineering Structures. 2019; 181:653-669.
26. Chakraborty S, Dey T, Kumar R. Stability and vibration analysis of CNT-Reinforced functionally graded laminated composite cylindrical shell panels using semi-analytical approach. Composites Part B: Engineering. 2019; 168:1-14.
27. Ebrahimi F, Dabbagh A, Civalek Ö. Vibration analysis of magnetically affected graphene oxide-reinforced nanocomposite beams. Journal of Vibration and Control. 2019; 25(23-24):2837-2849.
28. Ebrahimi F, Nouraei M, Dabbagh A, et al. Buckling analysis of graphene oxide powder-reinforced nanocomposite beams subjected to non-uniform magnetic field. Structural Engineering and Mechanics. 2019; 71(4):351-361.
29. Ebrahimi F, Nouraei M, Dabbagh A, et al. Thermal buckling analysis of embedded graphene-oxide powder-reinforced nanocomposite plates. Advances in Nano Research. 2019; 7(5):293-310.
30. Jiao P, Chen Z, Li Y, et al. Dynamic buckling analyses of functionally graded carbon nanotubes reinforced composite (FG-CNTRC) cylindrical shell under axial power-law time-varying displacement load. Composite Structures. 2019; 220:784-797.
31. Khosravi S, Arvin H, Kiani Y. Interactive thermal and inertial buckling of rotating temperature-dependent FG-CNT reinforced composite beams. Composites Part B: Engineering. 2019; 175:107178.
32. Kamarian S, Bodaghi M, Barbaz Isfahani R, et al. A comparison between the effects of shape memory alloys and carbon nanotubes on the thermal buckling of laminated composite beams. Mechanics Based Design of Structures and Machines. 2020:1-24.
33. Dat ND, Thanh NV, MinhAnh V, et al. Vibration and nonlinear dynamic analysis of sandwich FG-CNTRC plate with porous core layer. Mechanics of Advanced Materials and Structures. 2020:1-18.
34. Mahesh V, Harursampath D. Nonlinear deflection analysis of CNT/magneto-electro-elastic smart shells under multi-physics loading. Mechanics of Advanced Materials and Structures. 2020:1-25.
35. Safarpour M, Ghabussi A, Ebrahimi F, et al. Frequency characteristics of FG-GPLRC viscoelastic thick annular plate with the aid of GDQM. Thin-Walled Structures. 2020; 150:106683.
36. Civalek Ö, Avcar M. Free vibration and buckling analyses of CNT reinforced laminated non-rectangular plates by discrete singular convolution method. Engineering with Computers. 2020.
37. Shamsaddini Lori E, Ebrahimi F, Supeni EEB, et al. Frequency characteristics of a GPL-reinforced composite microdisk coupled with a piezoelectric layer. The European Physical Journal Plus. 2020; 135(2):144.
38. Moradi-Dastjerdi R, Behdinan K, Safaei B, et al. Buckling behavior of porous CNT-reinforced plates integrated between active piezoelectric layers. Engineering Structures. 2020; 222:111141.
39. Kamarian S, Bodaghi M, Barbaz Isfahani R, et al. Influence of carbon nanotubes on thermal expansion coefficient and thermal buckling of polymer composite plates: experimental and numerical investigations. Mechanics Based Design of Structures and Machines. 2021; 49(2):217-232.
40. Ebrahimi F, Hashemabadi D, Habibi M, et al. Thermal buckling and forced vibration characteristics of a porous GNP reinforced nanocomposite cylindrical shell. Microsystem Technologies. 2020; 26(2):461-473.
41. Shokrgozar A, Ghabussi A, Ebrahimi F, et al. Viscoelastic dynamics and static responses of a graphene nanoplatelets-reinforced composite cylindrical microshell. Mechanics Based Design of Structures and Machines. 2020:1-28.
42. Ganapathi M, Anirudh B, Anant C, et al. Dynamic characteristics of functionally graded graphene reinforced porous nanocomposite curved beams based on trigonometric shear deformation theory with thickness stretch effect. Mechanics of Advanced Materials and Structures. 2021; 28(7):741-752.

43. Amani MA, Ebrahimi F, Dabbagh A, et al. A machine learning-based model for the estimation of the temperature-dependent moduli of graphene oxide reinforced nanocomposites and its application in a thermally affected buckling analysis. Engineering with Computers. 2021; 37(3):2245-2255.
44. Kallannavar V, Kattimani S. Effect of temperature on the performance of active constrained layer damping of skew sandwich plate with CNT reinforced composite core. Mechanics of Advanced Materials and Structures. 2021:1-20.
45. Moradi Z, Davoudi M, Ebrahimi F, et al. Intelligent wave dispersion control of an inhomogeneous micro-shell using a proportional-derivative smart controller. Waves in Random and Complex Media. 2021:1-24.
46. Kamarian S, Bodaghi M, Barbaz Isfahani R, et al. Thermal buckling analysis of sandwich plates with soft core and CNT-Reinforced composite face sheets. Journal of Sandwich Structures & Materials. 2021; 23(8):3606-3644.
47. Zhang L, Chen Z, Habibi M, et al. Low-velocity impact, resonance, and frequency responses of FG-GPLRC viscoelastic doubly curved panel. Composite Structures. 2021; 269:114000.
48. Maji P, Rout M, Karmakar A. The free vibration response of temperature-dependent carbon nanotube-reinforced composite stiffened plate. Mechanics of Advanced Materials and Structures. 2021:1-15.
49. Zhang M, Li J. Carbon nanotube in different shapes. Materials Today. 2009; 12(6):12-18.
50. Ebrahimi F, Dabbagh A. A brief review on the influences of nanotubes' entanglement and waviness on the mechanical behaviors of CNTR polymer nanocomposites. Journal of Computational Applied Mechanics. 2020; 51(1):247-252.
51. Arasteh R, Omidi M, Rousta AHA, et al. A Study on Effect of Waviness on Mechanical Properties of Multi-Walled Carbon Nanotube/Epoxy Composites Using Modified Halpin–Tsai Theory. Journal of Macromolecular Science, Part B. 2011; 50(12):2464-2480.
52. García-Macías E, Rodríguez-Tembleque L, Castro-Triguero R, et al. Eshelby-Mori-Tanaka approach for post-buckling analysis of axially compressed functionally graded CNT/polymer composite cylindrical panels. Composites Part B: Engineering. 2017; 128:208-224.
53. Rafiee M, Liu XF, He XQ, et al. Geometrically nonlinear free vibration of shear deformable piezoelectric carbon nanotube/fiber/polymer multiscale laminated composite plates. Journal of Sound and Vibration. 2014; 333(14):3236-3251.
54. He XQ, Rafiee M, Mareishi S, et al. Large amplitude vibration of fractionally damped viscoelastic CNTs/fiber/polymer multiscale composite beams. Composite Structures. 2015; 131:1111-1123.
55. Rafiee M, Nitzsche F, Labrosse M. Rotating nanocomposite thin-walled beams undergoing large deformation. Composite Structures. 2016; 150:191-199.
56. Ebrahimi F, Habibi S. Nonlinear eccentric low-velocity impact response of a polymer-carbon nanotube-fiber multiscale nanocomposite plate resting on elastic foundations in hygrothermal environments. Mechanics of Advanced Materials and Structures. 2018; 25(5):425-438.
57. Rafiee M, Nitzsche F, Labrosse MR. Modeling and mechanical analysis of multiscale fiber-reinforced graphene composites: Nonlinear bending, thermal post-buckling and large amplitude vibration. International Journal of Non-Linear Mechanics. 2018; 103:104-112.
58. Ebrahimi F, Dabbagh A. Vibration analysis of graphene oxide powder-/carbon fiber-reinforced multi-scale porous nanocomposite beams: A finite-element study. The European Physical Journal Plus. 2019; 134(5):225.
59. Ebrahimi F, Dabbagh A, Rastgoo A, et al. Agglomeration Effects on Static Stability Analysis of Multi-Scale Hybrid Nanocomposite Plates. Computers, Materials & Continua. 2020; 63(1):41-64.
60. Ebrahimi F, Dabbagh A. Vibration analysis of multi-scale hybrid nanocomposite shells by considering nanofillers' aggregation. Waves in Random and Complex Media. 2020:1-19.
61. Dabbagh A, Rastgoo A, Ebrahimi F. Post-buckling analysis of imperfect multi-scale hybrid nanocomposite beams rested on a nonlinear stiff substrate. Engineering with Computers. 2020.
62. Dabbagh A, Rastgoo A, Ebrahimi F. Static stability analysis of agglomerated multi-scale hybrid nanocomposites via a refined theory. Engineering with Computers. 2021; 37(3):2225–2244.
63. Dabbagh A, Rastgoo A, Ebrahimi F. Thermal buckling analysis of agglomerated multiscale hybrid nanocomposites via a refined beam theory. Mechanics Based Design of Structures and Machines. 2021; 49(3):403-429.
64. Ebrahimi F, Dabbagh A. An analytical solution for static stability of multi-scale hybrid nanocomposite plates. Engineering with Computers. 2021; 37(1):545–559.
65. Ebrahimi F, Dabbagh A, Rastgoo A. Free vibration analysis of multi-scale hybrid nanocomposite plates with agglomerated nanoparticles. Mechanics Based Design of Structures and Machines. 2021; 49(4):487-510.

66. Ebrahimi F, Nopour R, Dabbagh A. Effect of viscoelastic properties of polymer and wavy shape of the CNTs on the vibrational behaviors of CNT/glass fiber/polymer plates. Engineering with Computers. 2021.
67. Ferry JD. Viscoelastic Properties of Polymers. 3rd ed.: John Wiley and Sons; 1980.
68. Drozdov AD, Kalamkarov AL. A constitutive model for nonlinear viscoelastic behavior of polymers. Polymer Engineering & Science. 1996; 36(14):1907-1919.
69. Brinson HF, Brinson LC. Polymer Engineering Science and Viscoelasticity. 2nd ed. Boston, MA: Springer; 2008.
70. Bacciocchi M, Tarantino AM. Time-dependent behavior of viscoelastic three-phase composite plates reinforced by Carbon nanotubes. Composite Structures. 2019; 216:20-31.
71. Cox HL. The elasticity and strength of paper and other fibrous materials. British Journal of Applied Physics. 1952; 3(3):72-79.
72. Zaoui FZ, Ouinas D, Tounsi A. New 2D and quasi-3D shear deformation theories for free vibration of functionally graded plates on elastic foundations. Composites Part B: Engineering. 2019; 159:231-247.
73. Lai WM, Krempl E, Rubin D. Introduction to Continuum Mechanics. 4th ed.: Elsevier; 2010.
74. Xu D, Liu Q, Qin Y, et al. Analytical approach for crack identification of glass fiber reinforced polymer–sea sand concrete composite structures based on strain dissipations. Structural Health Monitoring. 2020:1475921720974290.
75. Kabir H, Aghdam MM. A generalized 2D Bézier-based solution for stress analysis of notched epoxy resin plates reinforced with graphene nanoplatelets. Thin-Walled Structures. 2021; 169:108484.
76. Zhang W, Tang Z. Numerical Modeling of Response of CFRP–Concrete Interfaces Subjected to Fatigue Loading. Journal of Composites for Construction. 2021; 25(5):04021043.
77. Dabbagh A, Ebrahimi F. Postbuckling analysis of meta-nanocomposite beams by considering the CNTs' agglomeration. The European Physical Journal Plus. 2021; 136(11):1168.
78. Ebrahimi F, Nopour R, Dabbagh A. Smart laminates with an auxetic ply rested on visco-Pasternak medium: Active control of the system's oscillation. Engineering with Computers. 2021.
79. Huang H, Xue C, Zhang W, et al. Torsion design of CFRP-CFST columns using a data-driven optimization approach. Engineering Structures. 2022; 251:113479.
80. Dabbagh A, Rastgoo A, Ebrahimi F. Finite element vibration analysis of multi-scale hybrid nanocomposite beams via a refined beam theory. Thin-Walled Structures. 2019; 140:304-317.
81. Wattanasakulpong N, Ungbhakorn V. Analytical solutions for bending, buckling and vibration responses of carbon nanotube-reinforced composite beams resting on elastic foundation. Computational Materials Science. 2013; 71:201-208.
82. Zhang Z, Li Y, Wu H, et al. Mechanical analysis of functionally graded graphene oxide-reinforced composite beams based on the first-order shear deformation theory. Mechanics of Advanced Materials and Structures. 2020; 27(1):3-11.

Table 1 Initial mechanical properties of the polymeric matrix and glass fibers [70].

E_{PM}^{0}	2.1 GPa
ν_{PM}^{0}	0.34
ρ_{PM}^{0}	1150 kg/m^3
E_F	71 GPa
G_F	30 GPa
ν_F	0.22
ρ_F	2450 kg/m^3

Table 2 Material properties of SWCNT [56].

E_{CNT}	$640(1-0.0005\ \Delta T)$ GPa
d_{CNT}	1.4×10^{-9} m
t_{CNT}	0.34×10^{-9} m
ρ_{CNT}	1350 Kg/m^3
l_{CNT}	25×10^{-6} m
ν_{CNT}	0.33

Table 3 Natural frequency responses of CNTR nanocomposite beams (L/h=15)

Source	$V_{CNT}^{*}=0.12$	$V_{CNT}^{*}=0.17$	$V_{CNT}^{*}=0.28$
Ref. [9]	0.9753	1.1999	1.4401
Ref. [80]	0.9698	1.2030	1.4236
Present work	0.9628	1.1574	1.4348

Table 4 First dimensionless frequencies of CNTR nanocomposite beams (L/h=15, V_{CNT}=0.12)

	Distribution Type		
Source	UD	FG-O	FG-X
Ref. [81]	0.9976	0.7628	1.1485
Ref. [82]	0.9842	0.7595	1.1249
Present work	0.9904	0.7528	1.1399

List of Figures

Figure 1. Some of the applications of nanocomposite materials in the field of structural mechanics.

Figure 2. Variation of the first dimensionless frequency of multi-scale hybrid nanocomposite beams versus time for **(a)** S-S and **(b)** C-C BCs once the relaxation time is varied (m_f=0.2, m_r=0.05, C_w=0.35).

Figure 3. Variation of the first dimensionless frequency of multi-scale hybrid nanocomposite S-S beams fabricated from **(a)** straight CNTs and **(b)** wavy CNTs versus time once the mass fraction of the CNTs is varied (m_f=0.2).

Figure 4. Variation of the first dimensionless frequency of multi-scale hybrid nanocomposite S-S beams fabricated from **(a)** straight CNTs and **(b)** wavy CNTs versus time once the mass fraction of the GFs is varied (m_r=0.05).

Figure 5. Variation of the **(a)** first, **(b)** second, and **(c)** third dimensionless frequency of multi-scale hybrid nanocomposite S-S beams fabricated from wavy CNTs versus time once the waviness coefficient is varied (m_r=0.05, m_f=0.2).

Figure 1

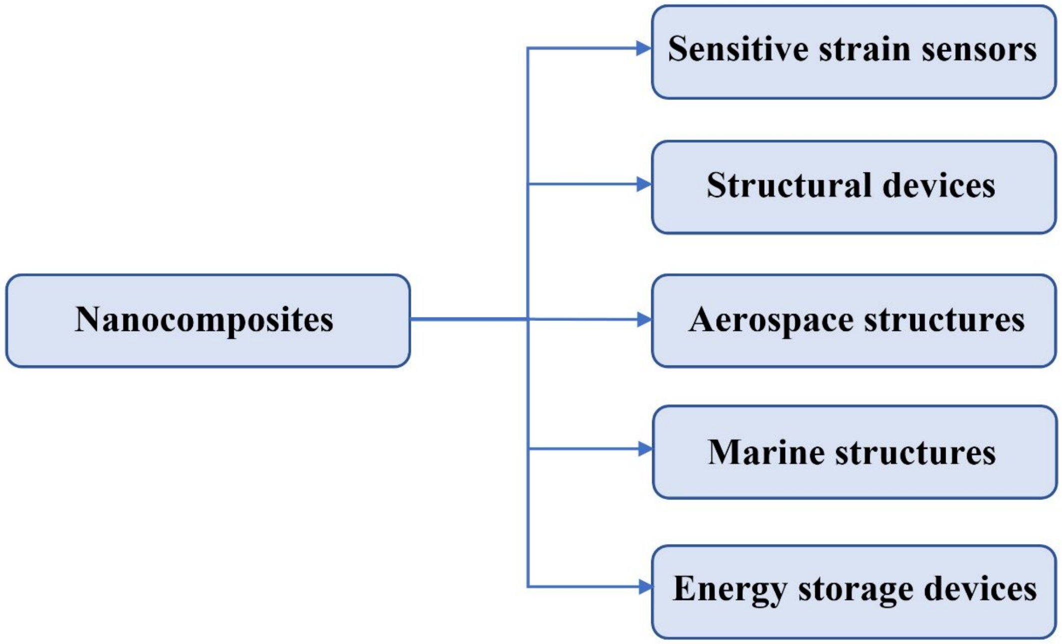
Nanocomposites
Sensitive strain sensors
Structural devices
Aerospace structures
Marine structures
Energy storage devices

Figure 2a

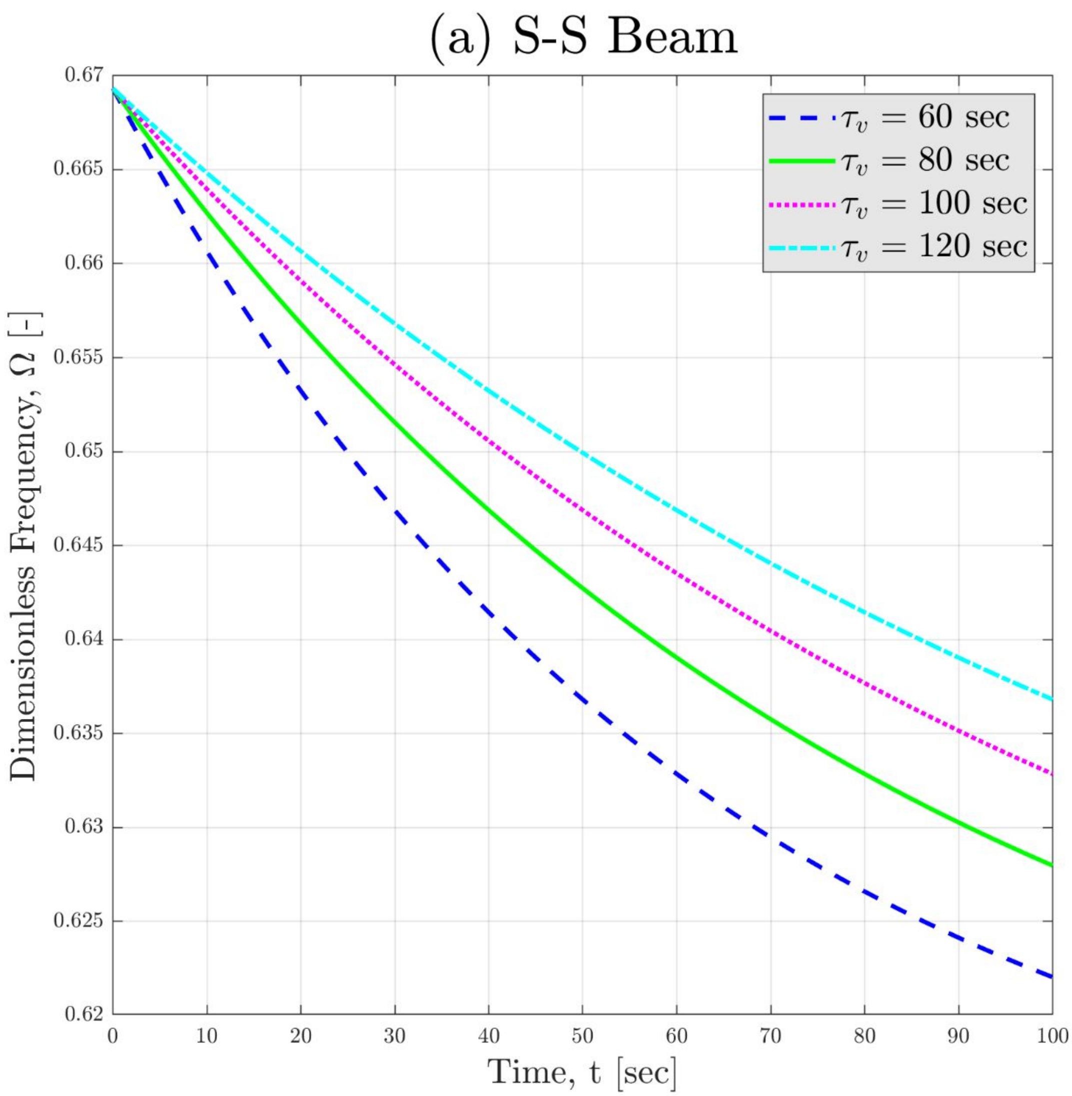
(a) S-S Beam
Dimensionless Frequency, Ω [-]
Time, t [sec]
$\tau_v = 60$ sec
$\tau_v = 80$ sec
$\tau_v = 100$ sec
$\tau_v = 120$ sec
0.67
0.665
0.66
0.655
0.65
0.645
0.64
0.635
0.63
0.625
0.62
0
10
20
30
40
50
60
70
80
90
100

Figure 2b

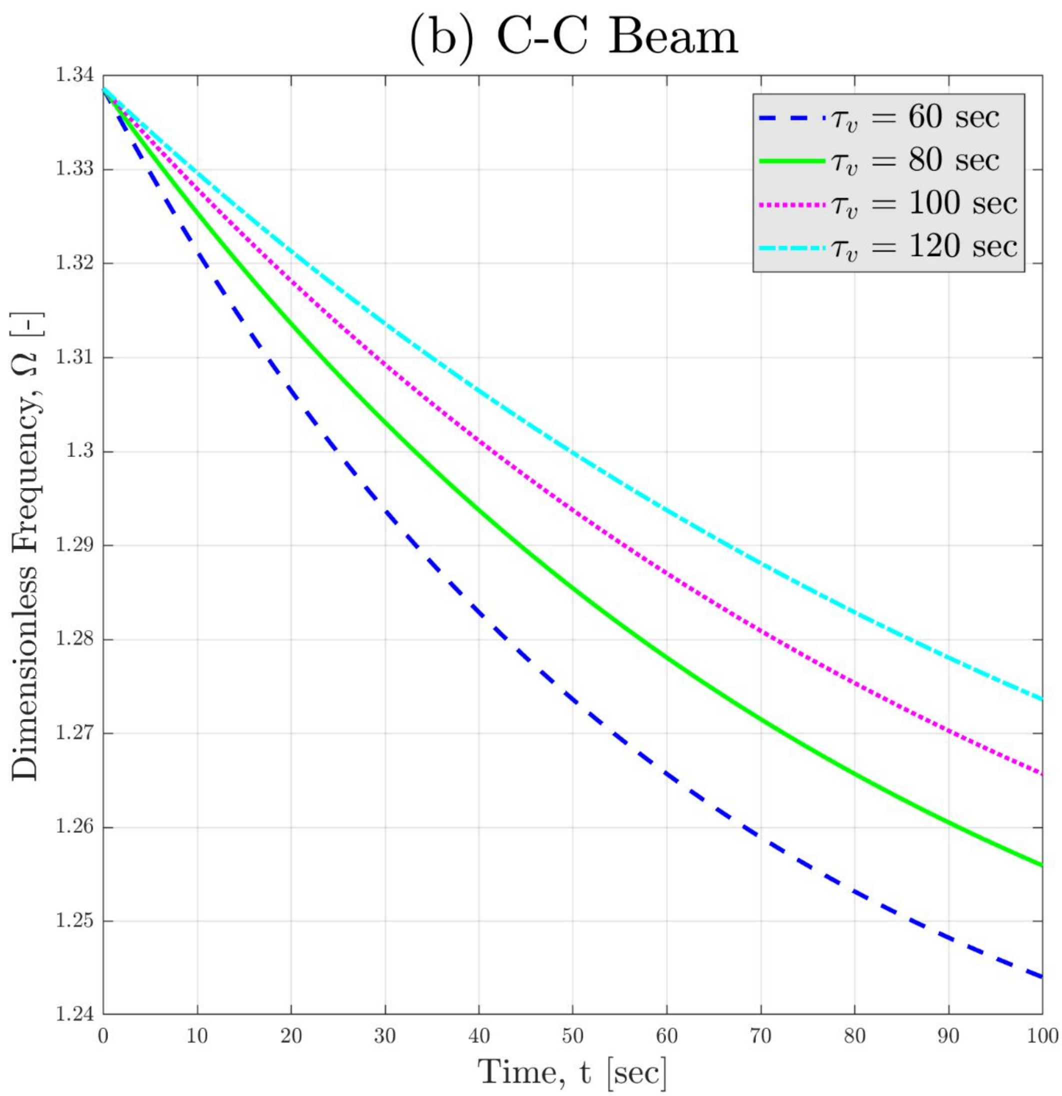
(b) C-C Beam
τ_v = 60 sec
τ_v = 80 sec
τ_v = 100 sec
τ_v = 120 sec
Dimensionless Frequency, Ω [-]
Time, t [sec]
1.34
1.33
1.32
1.31
1.3
1.29
1.28
1.27
1.26
1.25
1.24
0
10
20
30
40
50
60
70
80
90
100

Figure 3a

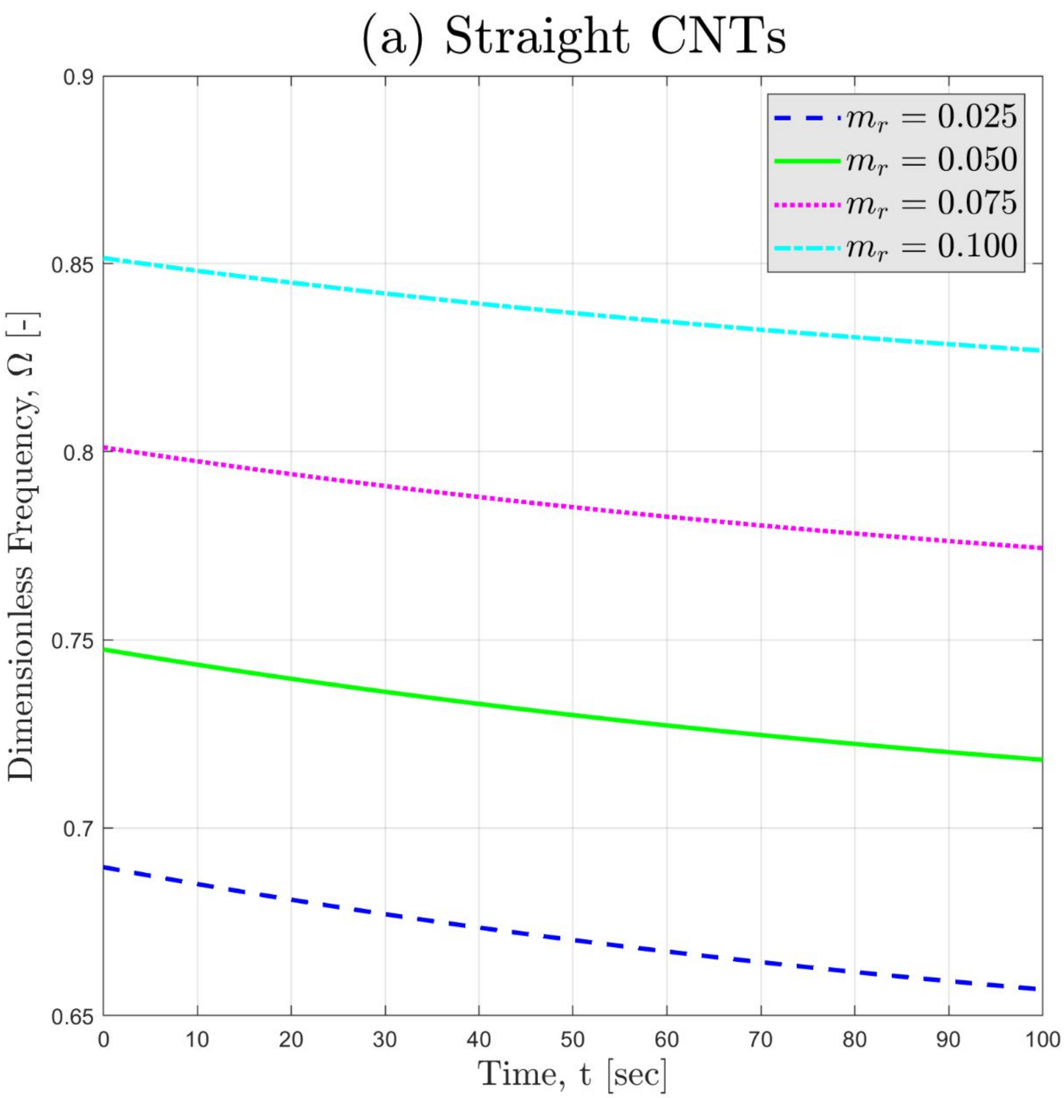
(a) Straight CNTs
$m_r = 0.025$
$m_r = 0.050$
$m_r = 0.075$
$m_r = 0.100$
Dimensionless Frequency, Ω [-]
Time, t [sec]
0.9
0.85
0.8
0.75
0.7
0.65
0
10
20
30
40
50
60
70
80
90
100

Figure 3b

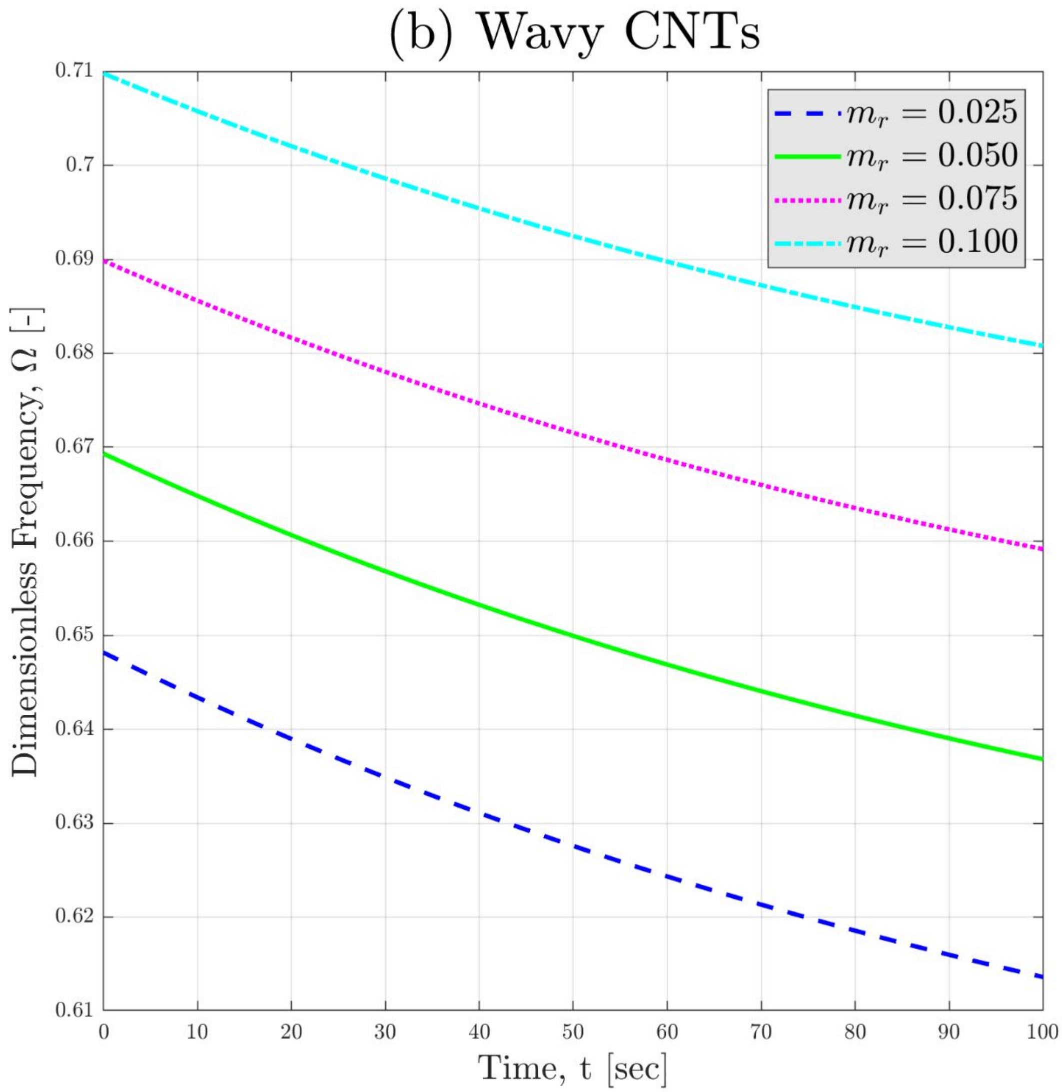
(b) Wavy CNTs
$m_r = 0.025$
$m_r = 0.050$
$m_r = 0.075$
$m_r = 0.100$
Dimensionless Frequency, Ω [-]
Time, t [sec]
0.71
0.7
0.69
0.68
0.67
0.66
0.65
0.64
0.63
0.62
0.61
0
10
20
30
40
50
60
70
80
90
100

Figure 4a

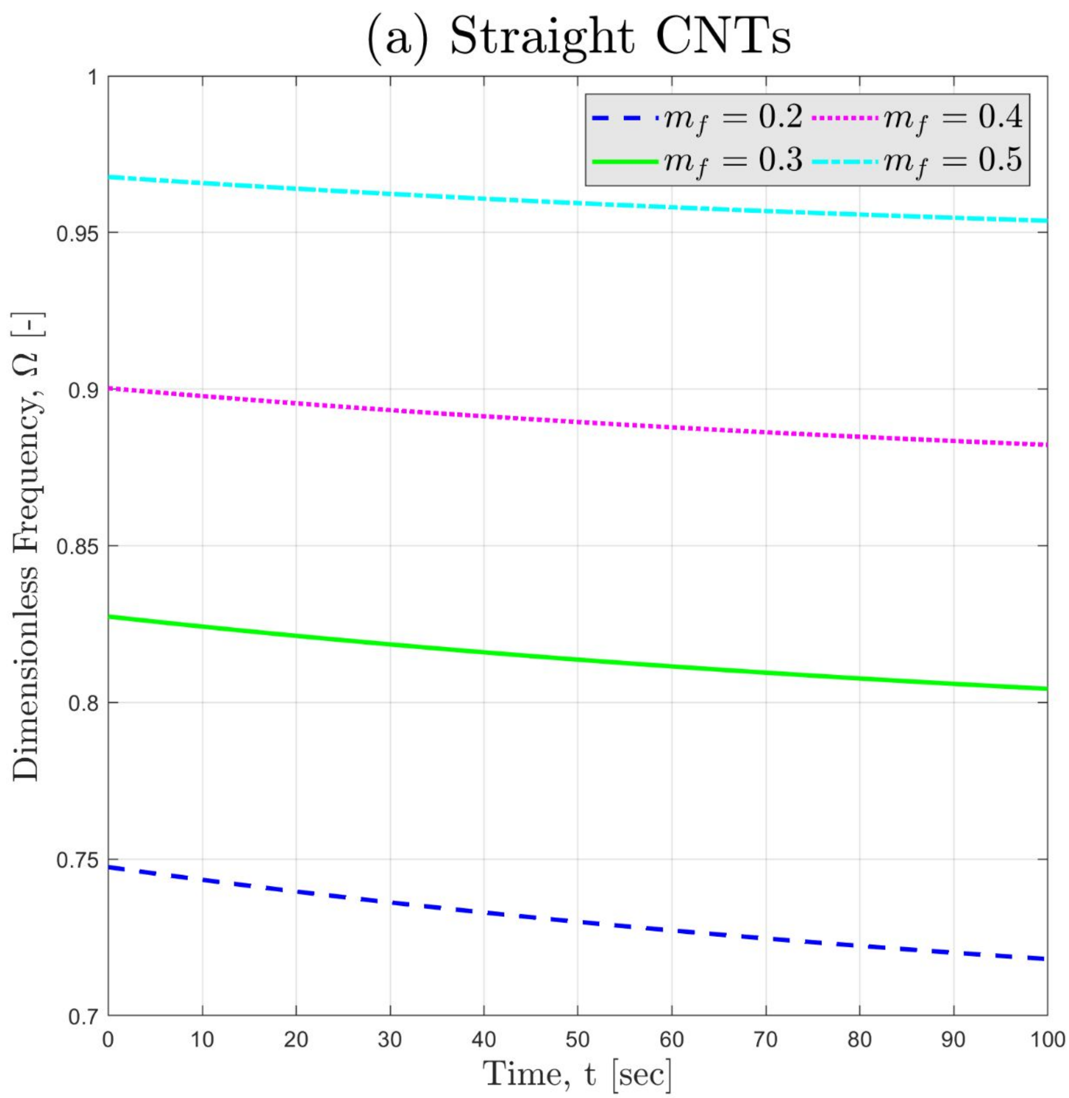
(a) Straight CNTs
$m_f = 0.2$
$m_f = 0.4$
$m_f = 0.3$
$m_f = 0.5$
Dimensionless Frequency, Ω [-]
Time, t [sec]
1
0.95
0.9
0.85
0.8
0.75
0.7
0
10
20
30
40
50
60
70
80
90
100

Figure 4b

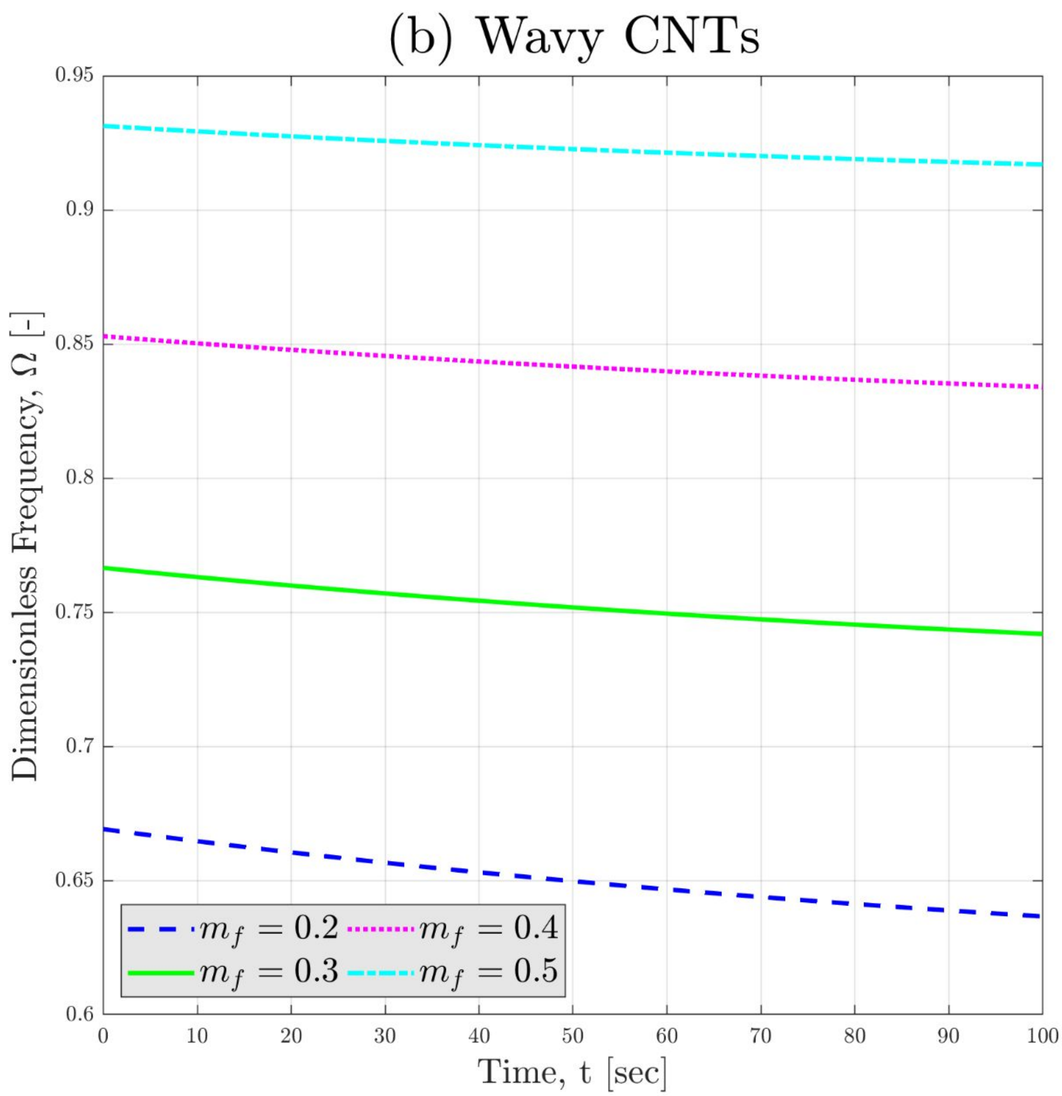

(b) Wavy CNTs
Dimensionless Frequency, Ω [-]
Time, t [sec]
0.95
0.9
0.85
0.8
0.75
0.7
0.65
0.6
0
10
20
30
40
50
60
70
80
90
100
$m_f = 0.2$
$m_f = 0.4$
$m_f = 0.3$
$m_f = 0.5$

Figure 5a

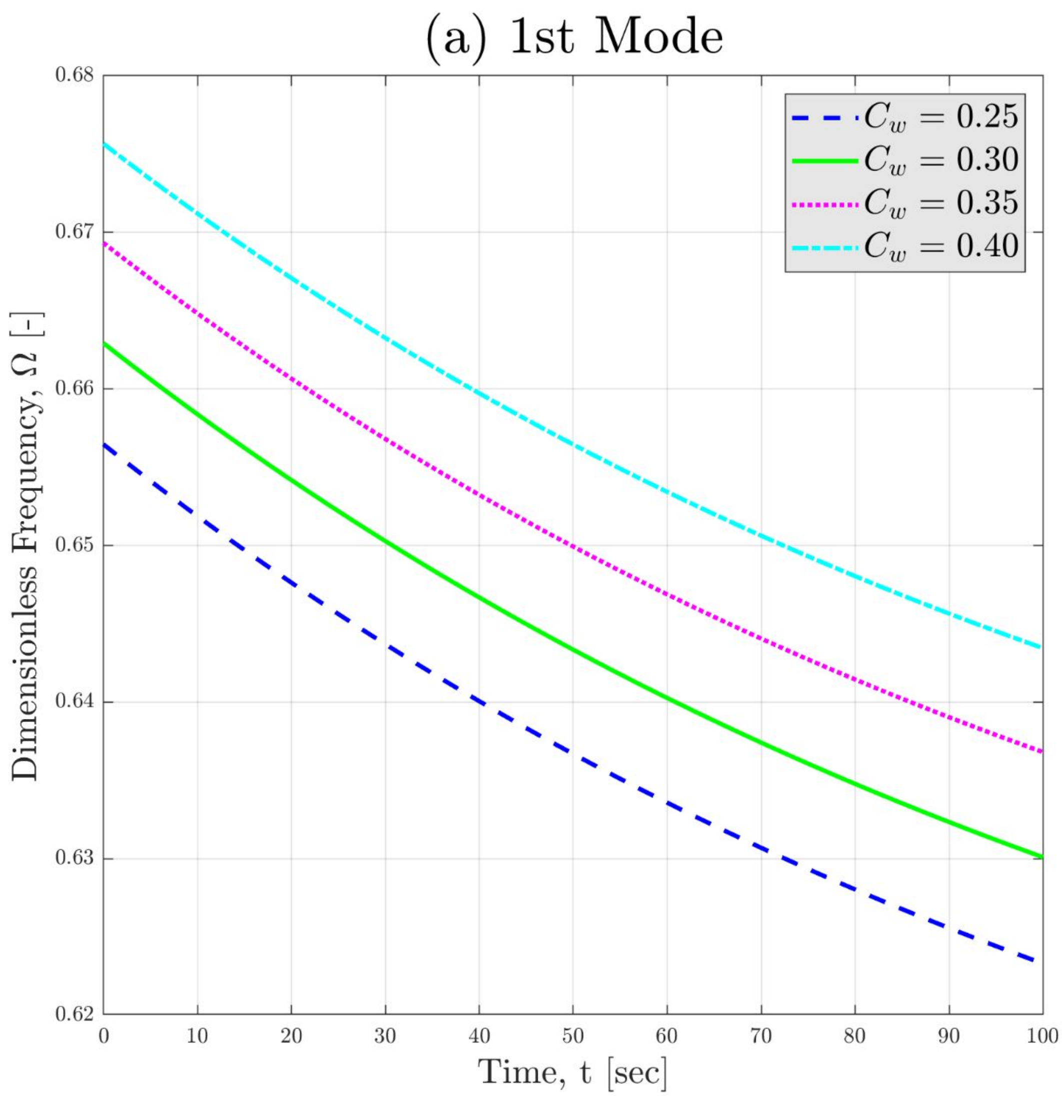
(a) 1st Mode
Dimensionless Frequency, Ω [-]
Time, t [sec]
0.68
0.67
0.66
0.65
0.64
0.63
0.62
0
10
20
30
40
50
60
70
80
90
100
$C_w = 0.25$
$C_w = 0.30$
$C_w = 0.35$
$C_w = 0.40$

Figure 5b

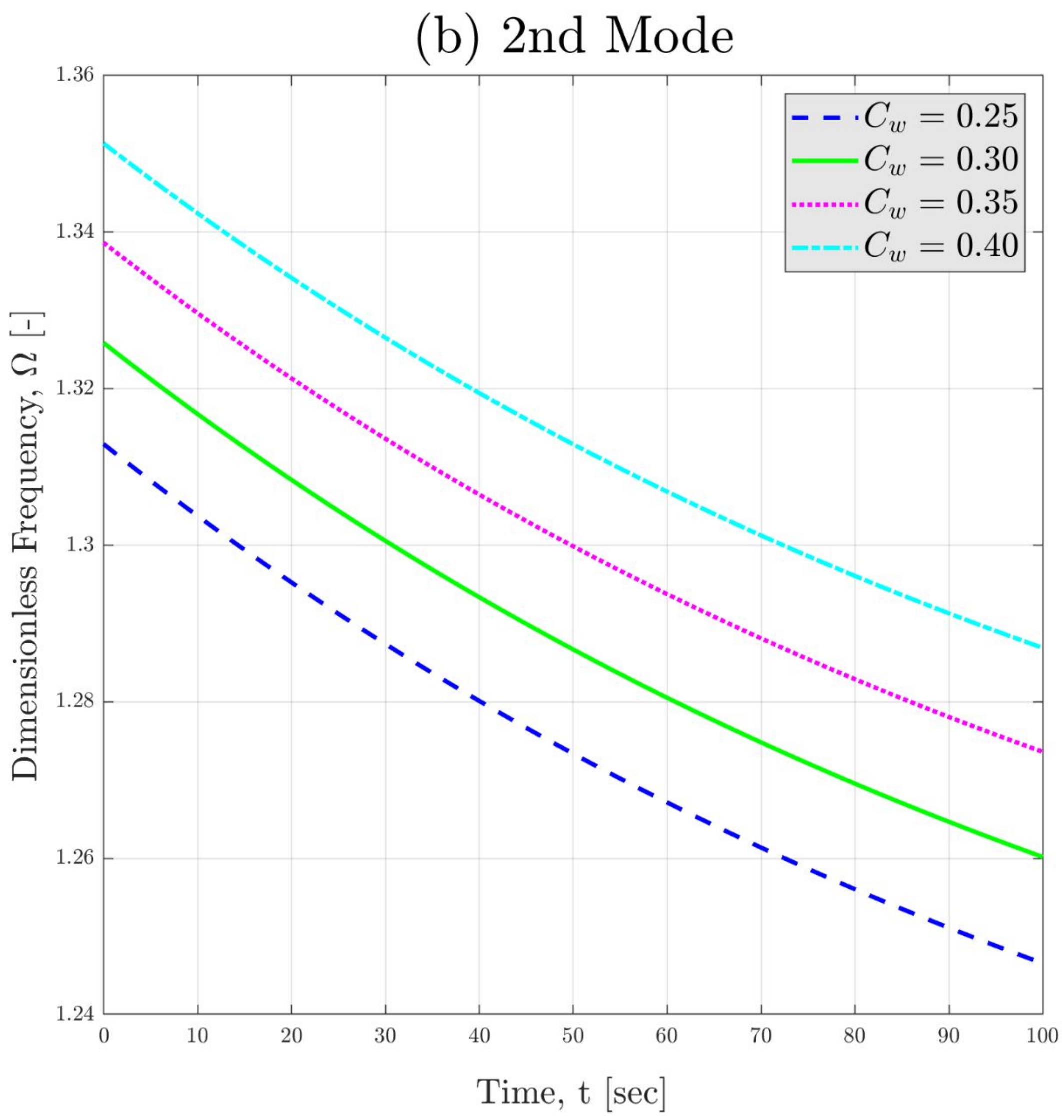
(b) 2nd Mode
$C_w = 0.25$
$C_w = 0.30$
$C_w = 0.35$
$C_w = 0.40$
Dimensionless Frequency, Ω [-]
Time, t [sec]
1.36
1.34
1.32
1.3
1.28
1.26
1.24
0
10
20
30
40
50
60
70
80
90
100

Figure 5c

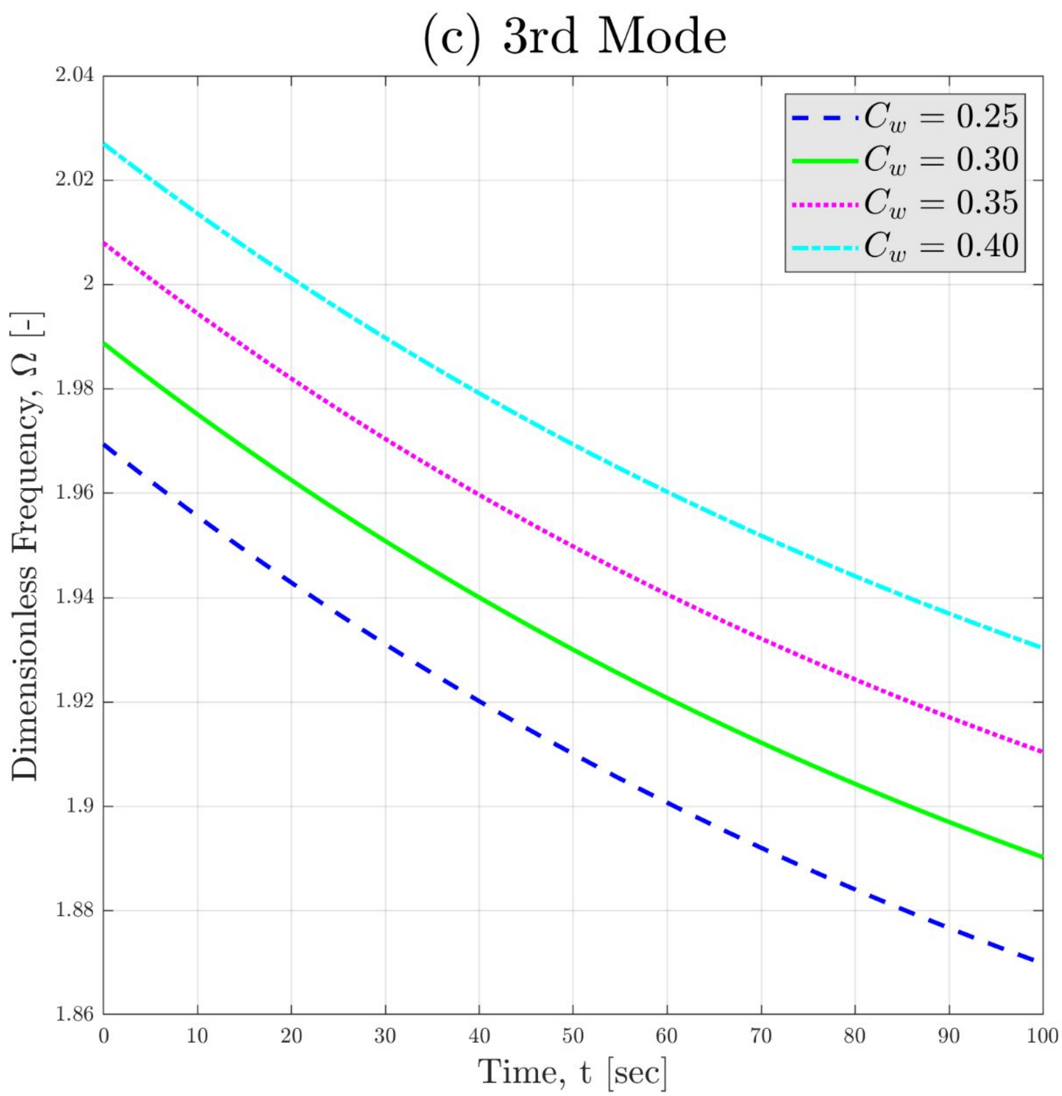
(c) 3rd Mode
Dimensionless Frequency, Ω [-]
Time, t [sec]
$C_w = 0.25$
$C_w = 0.30$
$C_w = 0.35$
$C_w = 0.40$
2.04
2.02
2
1.98
1.96
1.94
1.92
1.9
1.88
1.86
0
10
20
30
40
50
60
70
80
90
100